encit 2020

ABCM
Associação Brasileira de Engenharia e Ciências Mecânicas

18th Brazilian Congress of Thermal Sciences and Engineering
November 16–20, 2020 (Online)

ENC-2020-0318
EFFECTS OF THE BULK VISCOSITY COEFFICIENT IN UNSTEADY PIPE FLOW

André Luís Peixoto Considera
Felipe Bastos de Freitas Rachid
Universidade Federal Fluminense - UFF, Campus Praia Vermelha, Rua Passo da Pátria,156, 24210-240 Niterói, RJ, Brazil
e-mails: andreconsidera@id.uff.br, frachid@id.uff.br

Abstract. *The present study aims to investigate the effects of the bulk viscosity coefficient in unsteady pipe flow. To this end, a one-dimensional water-hammer model taking into account the bulk viscosity coefficient is developed by introducing its effects in the mass and momentum equations. The governing equations are solved by the method of characteristics (MOC) in a reservoir-pipe-valve system with transient generated by sudden valve closure. The effects of the bulk viscosity coefficient are numerically investigated regarding the pressure response as well as the energy dissipation. Results indicate that large values of the bulk viscosity coefficient lead to an increase in the pressure wave period. Moreover, the energy dissipation due to the bulk viscosity occurs in the form of high intensity peaks, easily exceeding the dissipation due to wall shear when large values of the bulk viscosity coefficient are considered.*

Keywords: *unsteady pipe flow, bulk viscosity coefficient, energy dissipation*

1. INTRODUCTION

Liquid transmission lines are subjected to severe pressure surges whenever abrupt changes in the velocity of the fluid occur, giving rise to a transient flow regime commonly known as “water-hammer”. Transient pressure waves can be the source of damage to hydraulic components or even the complete rupture of the pipeline, typically generated by valve slam. Despite of its destructive effects, controlled hydraulic transients can serve beneficial purposes, playing a role in leakage detection and acting as an inexpensive way to gather data for model calibration.

A precise assessment of the friction forces that arise during the water-hammer event is of crucial importance in order to obtain an accurate prediction of the hydrodynamic loadings endured by the system. In the one-dimensional transient modelling it is necessary to employ friction models in order to incorporate higher dimensional effects, such as the large velocity gradients near the pipe wall during the flow reversal. The steady friction model assumes that the friction forces during unsteady flow are the same as in steady flow, that is, the Darcy-Weisbach formula is employed even though the flow is no longer in steady state. It is widely known that such model underestimates the dissipative mechanisms, resulting in greater wave amplitude and less damping when compared to experimental data. Such flawed behavior impelled several researchers to develop unsteady friction models in order to obtain a more accurate prediction of the dissipative effects during transient flow. In the unsteady friction model an unsteady friction term is added to the balance equations, becoming one of the main focus of research in water-hammer modelling to this day. A wide variety of dissipative mechanisms is present during water-hammer phenomena and the unsteady models are given the difficult task of offering a proper treatment of all those mechanisms. Nonetheless, the bulk viscosity coefficient is never considered when developing such models despite having an important role in the realm of fluid mechanics (Rajagopal, 2013), especially in the propagation of high frequency acoustic waves as discussed in Buresti (2015) . In an attempt to investigate the effects of the bulk viscosity in water-hammer phenomena, Di Nucci and Spena (2016) treated the flow problem as an inverse problem in which the bulk viscosity coefficient becomes a parameter of the pipe-fluid system, whose value also depends on the pipe properties. In a similar fashion, Landry *et al.* (2012) developed a viscoelastic model in which the bulk viscosity was incorporated in a new viscoelastic parameter accounting for both fluid and pipe properties. In the work of Pezzinga (2003) a 2D model was employed to investigate the additional dissipation generated by the bulk viscosity coefficient, as a result of thermodynamic interactions between liquid and gas, for unsteady pipe flow with cavitation.

To the best of the authors’ knowledge the literature concerning the bulk viscosity effects in water-hammer phenomena is rather scarce, warranting further investigation. The purpose of this study is to investigate such effects in the water-hammer event by developing a one-dimensional model taking the bulk viscosity coefficient into account. New forms of the mass and momentum equations are derived and later solved by the method of characteristics (MOC). A numerical study is performed in a reservoir-pipe-valve system with water-hammer generated by sudden valve closure. Afterwards, the influence of the bulk viscosity coefficient is assessed regarding the pressure response and energy dissipation.

2. MODEL

In this section we develop the mass and momentum equations for unsteady pipe flow taking into account the bulk viscosity coefficient.

2.1 Governing Equations

For water-hammer in Newtonian fluids, the mass and momentum balance equations in a one-dimensional setting can be written as (Wylie *et al*.,1993):

$$\frac{1}{\rho}\frac{d\rho}{dt} + \frac{1}{A}\frac{dA}{dt} + \frac{\partial u}{\partial x} = 0, \tag{1}$$

$$\frac{du}{dt} - \frac{1}{\rho}\frac{\partial \sigma}{\partial x} + \tau_w \frac{P}{\rho A} + g\, sin\theta = 0, \tag{2}$$

where d/dt is the material derivative operator, ρ the density, A the pipe cross-section area, u the longitudinal velocity component, τ_w the wall shear, P the pipe perimeter, g the gravitational acceleration and θ the angle between the pipe center-line and the horizontal axis. The longitudinal stress component σ is the sum of the spherical and deviatoric parcels:

$$\sigma = \sigma_s + \sigma_d, \tag{3}$$

which are expressed as follows for a compressible Newtonian fluid:

$$\sigma_s = -p + \sigma_s^i, \quad \text{with } \sigma_s^i = \mu_b\, \text{div}(\boldsymbol{V}) = -\mu_b \left(\frac{1}{\rho}\frac{d\rho}{dt}\right), \tag{4}$$

$$\sigma_d = 2\mu\frac{\partial u}{\partial x} - \frac{2\mu}{3}\text{div}(\boldsymbol{V}) = 2\mu\frac{\partial u}{\partial x} + \frac{2\mu}{3}\left(\frac{1}{\rho}\frac{d\rho}{dt}\right), \tag{5}$$

where p is the thermodynamic pressure, σ_s^i the irreversible part of the spherical parcel, $\boldsymbol{V}$ the velocity vector, μ the dynamic viscosity and μ_b the bulk viscosity. The second equality in Eqs.(4.2) and (5) is due to the mass conservation principle, which allows us to write $\text{div}(\boldsymbol{V}) = -\frac{1}{\rho}\frac{d\rho}{dt}$. In assuming that the pipe has an uniform circular cross-section of area A_0 and that it is subjected to small deformation $\varepsilon_\theta \ll 1$, the cross-section area of the tube can be expressed in terms of the circumferential deformation of the pipe wall as:

$$A = A_0(1 + 2\varepsilon_\theta). \tag{6}$$

In addition, by restricting the analysis to thin-walled tubes ($R/e \geq 10$), the circumferential deformation can be expressed in terms of the spherical component of the stress as:

$$\varepsilon_\theta = \frac{R\psi}{eE}(-\sigma_s) = \frac{R\psi}{eE}(p - \sigma_s^i), \tag{7}$$

in which E stands for the Young modulus of the pipe material, R is the internal diameter of the pipe, e is the pipe thickness and ψ is a constant parameter related to the way the pipe is anchored. By taking the time derivative of the cross-section area given by Eq.(6) we get:

$$\frac{dA}{dt} = A_0\frac{2R\psi}{eE}\left(\frac{dp}{dt} - \frac{d\sigma_s^i}{dt}\right). \tag{8}$$

In assuming that the fluid behaves as a slightly compressible liquid ($p/K \ll 1$) undergoing isothermal transformations, the following equation of state can be considered:

$$\rho = \rho_0(1 + \frac{p}{K}), \tag{9}$$

where K is the bulk modulus of the liquid and ρ_0 its density in the unperturbed state. Taking the time derivative of Eq.(9) we get:

$$\frac{d\rho}{dt} = \frac{\rho_0}{K}\frac{dp}{dt}. \tag{10}$$

By taking Eqs.(8) and (10) into Eq.(1) we obtain:

$$\frac{1}{\rho_0 a^2}\frac{dp}{dt} - \frac{2R\psi}{eE}\frac{d\sigma_s^i}{dt} + \frac{\partial u}{\partial x} = 0, \tag{11}$$

where a stands for the wave front speed of the classical water-hammer problem in which the bulk viscosity has been disregarded:

$$a = \sqrt{\frac{K/\rho_0}{\left(1+\frac{2RK\psi}{eE}\right)}}. \tag{12}$$

By taking Eqs.(3), (4) and (5) into (2) we arrive at the following modified expression:

$$\frac{du}{dt} + \frac{1}{\rho_0}\frac{\partial p}{\partial x} - \frac{1}{\rho_0}\left[1 - \frac{2}{3}\frac{\mu}{\mu_b}\right]\frac{\partial \sigma_s^i}{\partial x} - \frac{2\mu}{\rho_0}\frac{\partial^2 u}{\partial x^2} + \tau_w \frac{P}{\rho_0 A_0} + g\, sin\theta = 0. \tag{13}$$

Finally, by taking Eq. (10) into Eq. (4.2) we obtain:

$$\frac{dp}{dt} + \frac{K}{\mu_b}\sigma_s^i = 0. \tag{14}$$

Equations (11), (13) and (14) form the governing equations for the water-hammer problem taking the bulk viscosity into account.

In order to classify this system of partial differential equations, we rewrite this system by substituting Eq.(14) into Eq. (11) to eliminate the term dp/dt:

$$\frac{d\sigma_s^i}{dt} - \frac{eE}{2R\psi}\frac{\partial u}{\partial x} + \frac{eE}{\mu_b 2R\psi}\left(1+\frac{2RK\psi}{eE}\right)\sigma_s^i = 0, \tag{15}$$

while also neglecting the convective terms in Eqs. (13), (14), (15) due to the low Mach number assumption (to be validated further ahead in the study):

$$\frac{\partial \sigma_s^i}{\partial t} - \frac{eE}{2R\psi}\frac{\partial u}{\partial x} + \frac{eE}{\mu_b 2R\psi}\left(1+\frac{2RK\psi}{eE}\right)\sigma_s^i = 0, \tag{16.1}$$

$$\frac{\partial u}{\partial t} + \frac{1}{\rho_0}\frac{\partial p}{\partial x} - \frac{1}{\rho_0}\left[1 - \frac{2}{3}\frac{\mu}{\mu_b}\right]\frac{\partial \sigma_s^i}{\partial x} - \frac{2\mu}{\rho_0}\frac{\partial^2 u}{\partial x^2} + \tau_w \frac{P}{\rho_0 A_0} + g\, sin\theta = 0, \tag{16.2}$$

$$\frac{\partial p}{\partial t} + \frac{K}{\mu_b}\sigma_s^i = 0. \tag{16.3}$$

The system given by Eqs.(16) can be written in the following canonical form:

$$\frac{\partial \boldsymbol{U}}{\partial t} + \boldsymbol{A}\frac{\partial \boldsymbol{U}}{\partial x} = \boldsymbol{S}\left(\boldsymbol{U}\right), \tag{17}$$

where $\boldsymbol{U} = \begin{bmatrix}\sigma_s^i & u & p\end{bmatrix}^{\mathrm{T}} \in \mathbb{R}^3$ and the matrix $\boldsymbol{A} \in \mathbb{R}^{3\times 3}$ and the source vector $\boldsymbol{S} \in \mathbb{R}^3$ are such that:

$$\boldsymbol{A} = \begin{bmatrix} 0 & -\frac{eE}{2R\psi} & 0 \\ -\frac{1}{\rho_0}\left[1-\frac{2}{3}\frac{\mu}{\mu_b}\right] & 0 & \frac{1}{\rho_0} \\ 0 & 0 & 0 \end{bmatrix} \quad ; \quad \boldsymbol{S}\left(\boldsymbol{U}\right) = \begin{bmatrix} -\frac{eE}{\mu_b 2R\psi}\left(1+\frac{2RK\psi}{eE}\right)\sigma_s^i \\ \frac{2\mu}{\rho_0}\frac{\partial^2 u}{\partial x^2} - \tau_w\frac{P}{\rho_0 A_0} - g\, sin\theta \\ -\frac{K}{\mu_b}\sigma_s^i \end{bmatrix}. \tag{18}$$

To mathematically classify the first-order system of the homogeneous parcel of the system of PDEs given by Eq.(17) we must assess the eigenvalues and eigenvectors of the matrix $\boldsymbol{A}$. The eigenvalues are given by the following characteristic equation,

$$\det(\boldsymbol{A} - \lambda \boldsymbol{I}) = 0, \tag{19}$$

whose straightforward solution gives three distinct values in increasing order:

$$\lambda_1 = -a^* \quad ; \quad \lambda_2 = 0 \quad ; \quad \lambda_3 = +a^* \quad \text{with} \quad a^* = \sqrt{\frac{eE}{\rho_0 2R\psi}\left[1-\frac{2}{3}\frac{\mu}{\mu_b}\right]}. \tag{20}$$

According to Eq.(20), in order to ensure real eigenvalues we must have:

$$\frac{\mu}{\mu_b} \leq \frac{3}{2}, \tag{21}$$

which seems to be in agreement with experimental results reported in the literature (Dukhin and Goetz, 2009). Subjecting the system to the restriction given by Eq. (21), the value of a^* represents the speed of the wave front with which disturbances propagate in the medium. It is worth mentioning that, in contrast to the classical water-hammer theory, the speed of the wave front a^* surprisingly does not depend on the bulk modulus of the liquid, as observed in Eq. (12). In an attempt to establish a close relationship with the wave speed a , we conveniently rewrite Eq. (20.4) as follows:

$$a^* = \sqrt{\frac{KeE}{K\rho_0 2R\psi}\left[1-\frac{2}{3}\frac{\mu}{\mu_b}\right]} = a\sqrt{\left(1+\frac{eE}{2RK\psi}\right)\left[1-\frac{2}{3}\frac{\mu}{\mu_b}\right]}. \tag{22}$$

Equation (22) shows that for typical values of the system parameters we have $a^* > a$, meaning that in such cases the wave front moves faster when considering the bulk viscosity coefficient. The next step towards the classification of the system of PDEs given by Eq.(17) is to compute the left eigenvectors $\boldsymbol{l}^{(i)}$ associated with λ_i for $i \in \{1,2,3\}$, which are defined as follows:

$$\boldsymbol{l}^{(i)}\boldsymbol{A} = \lambda_i \boldsymbol{l}^{(i)}, \text{for } i \in \{1,2,3\}. \tag{23}$$

Straightforward computations yield, without loss of generality:

$$\boldsymbol{l}^{(1)} = \left[+\frac{2R\psi a^*}{Ee} \quad 1 \quad -\frac{1}{\rho_0 a^*}\right], \tag{24.1}$$

$$\boldsymbol{l}^{(2)} = [0 \quad 0 \quad 1], \tag{24.2}$$

$$\boldsymbol{l}^{(3)} = \left[-\frac{2R\psi a^*}{Ee} \quad 1 \quad +\frac{1}{\rho_0 a^*}\right]. \tag{24.3}$$

Since $\boldsymbol{l}^{(i)}$ given by Eqs.(24) form a set of linear independent vectors spanning the space $\mathbb{R}^3$ and λ_i are all real, the system of PDEs given by Eq. (17) is hyperbolic.

2.2 Dimensional Analysis

We now turn our attention to the dimensional analysis of Eqs.(13), (14), (15) in an attempt to get a better understanding of the order of magnitude of each term in the equations. The dimensional variables are normalized as follows:

$$x^+ = x/D; \quad t^+ = t/(D/a^*); \quad p^+ = p/p_r; \quad u^+ = u/U; \quad (\sigma_s^i)^+ = \sigma_s^i/p_r; \quad \tau_w^+ = \tau_w/\tau_{ws}; \quad g^+ = g/(U^2/D) \tag{25}$$

where D is the initial pipe diameter, U the steady state velocity, $p_r = \rho_0 a^* U$ and $\tau_{ws} = f\rho_0 U|U|/8$, in which f stands for the Darcy-Weisbach friction factor. This choice of normalization results in the following set of non-dimensional equations:

$$\frac{\partial(\sigma_s^i)^+}{\partial t^+} + \mathrm{Ma}u^+\frac{\partial(\sigma_s^i)^+}{\partial x^+} - \left(1+\frac{eE}{2RK\psi}\right)\left(\frac{a}{a^*}\right)^2\frac{\partial u^+}{\partial x^+} + \left(1+\frac{eE}{2RK\psi}\right)\frac{KD}{\mu_b a^*}(\sigma_s^i)^+ = 0, \tag{26.1}$$

$$\frac{\partial u^+}{\partial t^+} + \mathrm{Ma}u^+\frac{\partial u^+}{\partial x^+} + \frac{\partial p^+}{\partial x^+} - \left[1-\frac{2}{3}\frac{\mu}{\mu_b}\right]\frac{\partial(\sigma_s^i)^+}{\partial x^+} - \frac{2\mathrm{Ma}}{\mathrm{Re}}\frac{\partial^2 u^+}{\partial(x^+)^2} + \frac{f}{2}\mathrm{Ma}\tau_w^+ + \mathrm{Ma}g^+ sin\theta = 0, \tag{26.2}$$

$$\frac{\partial p^+}{\partial t^+} + \mathrm{Ma}u^+\frac{\partial p^+}{\partial x^+} + \frac{KD}{\mu_b a^*}(\sigma_s^i)^+ = 0, \tag{26.3}$$

in which Re and Ma are the Reynolds and Mach numbers:

$$\mathrm{Re} = \frac{\rho_0 U D}{\mu} \quad ; \quad \mathrm{Ma} = \frac{U}{a^*}. \tag{27}$$

If the variables in Eqs.(25) are properly scaled, then for large Reynolds and small Mach numbers the convective terms can indeed be neglected, together with the second-order derivative in Eq.(16.2).

2.3 Clausius-Duhem Inequality

Lastly, we introduce the Clausius-Duhem inequality that will later be utilized to perform the energy analysis. We aim to assess the energy dissipated by the fluid due to both wall shear and bulk viscosity effects. To this end, we make use of the Clausius-Duhem inequality, which is an alternative way of expressing the second law of thermodynamics. The Clausius-Duhem inequality, as derived in Gonzaga Filho (2017), has the following formulation in the context of one-dimensional transient flow:

$$d_i := \frac{2u\tau_w}{R} + \frac{(\sigma_s^i)^2}{\mu_b} + \sigma_d\frac{du}{dx} \geq 0, \tag{28}$$

where d_i represents the local rate of energy dissipation per unit volume, with $d_s := 2u\tau_w/R$ representing the energy dissipation due to wall shear, whereas $d_b := (\sigma_s^i)^2/\mu_b$ represents the energy dissipation due to bulk viscosity effects.

3. METHOD OF CHARACTERISTICS

We consider a simple framework comprised of a upstream reservoir, a horizontal pipe ($sin\theta = 0$) and a downstream valve, with water-hammer generated by a sudden valve closure. In this setting the source term in Eq.(17) takes the form:

$$\boldsymbol{S}\left(\boldsymbol{U}\right) = \begin{bmatrix} -\frac{eE}{\mu_b 2R\psi}\left(1+\frac{2RK\psi}{eE}\right)\sigma_s^i \\ -\tau_w \frac{P}{\rho_0 A_0} \\ -\frac{K}{\mu_b}\sigma_s^i \end{bmatrix} \tag{29}$$

where we dropped the higher order derivative in view of the dimensional analysis. The system given by Eq.(17) with source term given by Eq.(29) can be readily solved by the MOC, which transforms the system of PDEs into a system of ODEs along its characteristic lines, yielding the following compatibility equations:

$$\mathrm{C}^+ : -\frac{2R\psi a^*}{Ee}\frac{d\sigma_s^i}{dt} + \frac{du}{dt} + \frac{1}{\rho_0 a^*}\frac{dp}{dt} + \tau_w\frac{P}{\rho_0 A} - \left(\frac{a^*}{\mu_b}\left(1+\frac{2RK\psi}{Ee}\right) - \frac{K}{\rho_0 a^* \mu_b}\right)\sigma_s^i = 0 \text{ along } \frac{dx}{dt} = +a^*, \tag{30.1}$$

$$\mathrm{C}^- : \frac{2R\psi a^*}{Ee}\frac{d\sigma_s^i}{dt} + \frac{du}{dt} - \frac{1}{\rho_0 a^*}\frac{dp}{dt} + \tau_w\frac{P}{\rho_0 A} + \left(\frac{a^*}{\mu_b}\left(1+\frac{2RK\psi}{Ee}\right) - \frac{K}{\rho_0 a^* \mu_b}\right)\sigma_s^i = 0 \text{ along } \frac{dx}{dt} = -a^*, \tag{30.2}$$

$$\mathrm{C}^0 : \frac{dp}{dt} + \frac{K}{\mu_b}\sigma_s^i = 0 \text{ along } \frac{dx}{dt} = 0. \tag{30.3}$$

We aim to obtain the solution in a discrete domain given by $x_{j+1} = x_j + \Delta x$ and $t^{n+1} = t^n + \Delta t$, with $\Delta t = \Delta x/a^*$ and $\Delta x = L/N$, in which L is the pipe length and N is the number of intervals originated from the spatial discretization. Integrating each compatibility equation along its characteristic line results in:

$$\begin{aligned}\mathrm{C}^+ : &-\frac{2R\psi a^*}{Ee}([\sigma_s^i]_j^{n+1} - [\sigma_s^i]_{j-1}^n) + (u_j^{n+1} - u_{j-1}^n) + \frac{1}{\rho_0 a^*}(p_j^{n+1} - p_{j-1}^n) + \frac{P}{8A}\int_{t^n}^{t^{n+1}} fu|u|dt \\ &- \left(\frac{a^*}{\mu_b}\left(1+\frac{2RK\psi}{Ee}\right) - \frac{K}{\rho_0 a^* \mu_b}\right)\int_{t^n}^{t^{n+1}} \sigma_s^i dt = 0,\end{aligned} \tag{31}$$

$$\begin{aligned}\mathrm{C}^- : &\frac{2R\psi a^*}{Ee}([\sigma_s^i]_j^{n+1} - [\sigma_s^i]_{j+1}^n) + (u_j^{n+1} - u_{j+1}^n) - \frac{1}{\rho_0 a^*}(p_j^{n+1} - p_{j+1}^n) + \frac{P}{8A}\int_{t^n}^{t^{n+1}} fu|u|dt \\ &+ \left(\frac{a^*}{\mu_b}\left(1+\frac{2RK\psi}{Ee}\right) - \frac{K}{\rho_0 a^* \mu_b}\right)\int_{t^n}^{t^{n+1}} \sigma_s^i dt = 0,\end{aligned} \tag{32}$$

$$\mathrm{C}^0 : (p_j^{n+1} - p_j^n) + \frac{K}{\mu_b}\int_{t^n}^{t^{n+1}} \sigma_s^i dt = 0, \tag{33}$$

where we used the steady friction model for the wall shear $\tau_w = f\rho_0 u|u|/8$. In order to deal with the integrals in Eqs.(31), (32), (33) we make use of numerical approximations:

$$\int_{t^n}^{t^{n+1}} fu|u|dt \approx \left(u_{j\pm1}^n + \epsilon(u_j^{n+1} - u_{j\pm1}^n)\right) f_{j\pm1}^n \left|u_{j\pm1}^n\right| \Delta t, \tag{34}$$

$$\int_{t^n}^{t^{n+1}} \sigma_s^i dt \approx \left(\theta[\sigma_s^i]_j^{n+1} + (1-\theta)[\sigma_s^i]_{j\pm1}^n\right)\Delta t, \tag{35}$$

in which $\theta \in [0,1]$ and ϵ is an approximation parameter, which we set as $\epsilon = 0.81$ in order to obtain a better approximation (Ghidaoui *et al.*, 2005). Subscripts $+$ and $-$ refer to C^- and C^+, respectively. For the characteristic C^0 we use:

$$\int_{t^n}^{t^{n+1}} \sigma_s^i dt \approx \left(\theta[\sigma_s^i]_j^{n+1} + (1-\theta)[\sigma_s^i]_j^n\right)\Delta t. \tag{36}$$

Substituting Eqs.(34), (35),(36) into Eqs.(31), (32), (33) we obtain a linear system of equations for each interior grid point, which we aim to solve for $[\sigma_s^i]_j^{n+1}$, u_j^{n+1} and p_j^{n+1}:

$$\mathrm{C}^+ : -(\alpha+\beta\theta\Delta t)[\sigma_s^i]_j^{n+1} + \left(1+\epsilon\Gamma^-\right)u_j^{n+1} + \frac{1}{\rho_0 a^*}p_j^{n+1} + \xi^- = 0, \tag{37.1}$$

$$\mathrm{C}^- : (\alpha+\beta\theta\Delta t)[\sigma_s^i]_j^{n+1} + \left(1+\epsilon\Gamma^+\right)u_j^{n+1} - \frac{1}{\rho_0 a^*}p_j^{n+1} + \xi^+ = 0, \tag{37.2}$$

$$\mathrm{C}^0 : \frac{K\theta\Delta t}{\mu_b}[\sigma_s^i]_j^{n+1} + p_j^{n+1} + \xi^0 = 0, \tag{37.3}$$

where the constants α and β together with the coefficients $\Gamma^\pm$, $\xi^\pm$ and ξ^0 are defined as follows:

$$\alpha = \frac{2R\psi a^*}{Ee}, \tag{38.1}$$

$$\beta = \frac{a^*}{\mu_b}\left(1+\frac{2RK\psi}{Ee}\right) - \frac{K}{\rho_0 a^* \mu_b}, \tag{38.2}$$

$$\Gamma^\pm = \frac{\Delta t}{4R} f_{j\pm1}^n \left|u_{j\pm1}^n\right|, \tag{38.3}$$

$$\xi^\pm = \pm[\beta\Delta t(1-\theta)-\alpha][\sigma_s^i]_{j\pm1}^n + [\Gamma^\pm(1-\epsilon)-1]u_{j\pm1}^n \pm \left(\frac{1}{\rho_0 a^*}\right)p_{j\pm1}^n, \tag{38.4}$$

$$\xi^0 = \frac{K\Delta t}{\mu_b}(1-\theta)[\sigma_s^i]_j^n - p_j^n. \tag{38.5}$$

Direct computations yield the following solution for the linear system comprised of Eqs. (37):

$$[\sigma_s^i]_j^{n+1} = \frac{-\xi^+(1+\epsilon\Gamma^-) + \xi^-(1+\epsilon\Gamma^+) - \frac{\xi^0}{\rho_0 a^*}(2+\epsilon(\Gamma^-+\Gamma^+))}{(2+\epsilon(\Gamma^-+\Gamma^+))(\alpha+(\beta+\frac{K}{\rho_0 a^* \mu_b})\theta\Delta t)}, \tag{39.1}$$

$$u_j^{n+1} = -\frac{\xi^- + \xi^+}{2+\epsilon(\Gamma^-+\Gamma^+)}, \tag{39.2}$$

$$p_j^{n+1} = \frac{\frac{K\Delta t\theta}{\mu_b}(\xi^+(1+\epsilon\Gamma^-) - \xi^-(1+\epsilon\Gamma^+)) - \xi^0(\alpha+\beta\theta\Delta t)(2+\epsilon(\Gamma^-+\Gamma^+))}{(2+\epsilon(\Gamma^-+\Gamma^+))(\alpha+(\beta+\frac{K}{\rho_0 a^* \mu_b})\theta\Delta t)}. \tag{39.3}$$

Eqs.(39) allow us to advance the solution from the time level t^n to t^{n+1} at each interior grid point. However, in order to solve for the boundary, one needs to introduce suitable boundary conditions.

3.1 Boundary Conditions

For a simple reservoir-pipe-valve system with a sudden valve closure, the spherical component of the stress is set to be a constant at the upstream reservoir, whereas a zero velocity condition is imposed at the downstream valve, i.e:

$$-p_{\text{res}}^{n+1} + [\sigma_s^i]_{\text{res}}^{n+1} = \text{const.} \quad ; \quad u_{\text{valve}}^{n+1} = 0, \tag{40}$$

where the subscripts 'res' and 'valve' refer to the reservoir and the valve. Therefore, by solving the linear system comprised of Eqs.(37.2), (37.3) and Eq.(40.1) we obtain the solution at the reservoir, whereas the solution at the valve is obtained by solving the linear system comprised of Eqs.(37.1), (37.3) and Eq.(40.2).

3.2 Initial Condition

The initial values of the relevant quantities are taken to be the steady-state values, which can be obtained by setting $\partial\sigma_s^i/\partial t = \partial u/\partial t = \partial p/\partial t = 0$ in Eqs.(16), which in turn yields the same steady-state as in the classical water-hammer theory, i.e, $[\sigma_s^i]_j^0 = 0$. This allows us to determine the steady-state values by following the same procedures and formulae found in most common literature, such as Wylie *et al.* (1993) and Chaudhry (1979):

$$U = \frac{C_d A_g}{\pi R^2}\sqrt{2gJ_v}, \tag{41.1}$$

$$p_j^0 = p_{\text{res}}^0 - \frac{\rho_0 f^0 U|U|}{2D}(x_j - x_{\text{res}}), \tag{41.2}$$

in which the superscript 0 denotes steady-state values, C_d is the discharge coefficient, A_g the area of the valve opening and J_v is the steady-state head loss across the valve.

4. RESULTS AND DISCUSSION

In this section we present the results obtained in the study together with a discussion of the general features of the model. We focus our analysis on the pressure response and on the energy dissipation due to both shear and bulk viscosity effects. We also wish to compare the results for different working fluids exhibiting large and small values of the bulk viscosity coefficient, for this reason we take benzene and water to be our test cases (Dukhin and Goetz, 2009).

4.1 Wave Speed

We start by employing Eq.(22) in order to compare the ratio between wave speeds a^*/a for different values of the ratio e/R. Figure 1 shows that the wave speed ratio gets closer to the unity as the values of e/R get smaller, which means the wave speed taking into account the bulk viscosity is similar to that of the classical water-hammer theory when considering pipes with very thin walls. It also shows that the discrepancies between wave speeds are more prominent for fluids with large values of bulk viscosity.

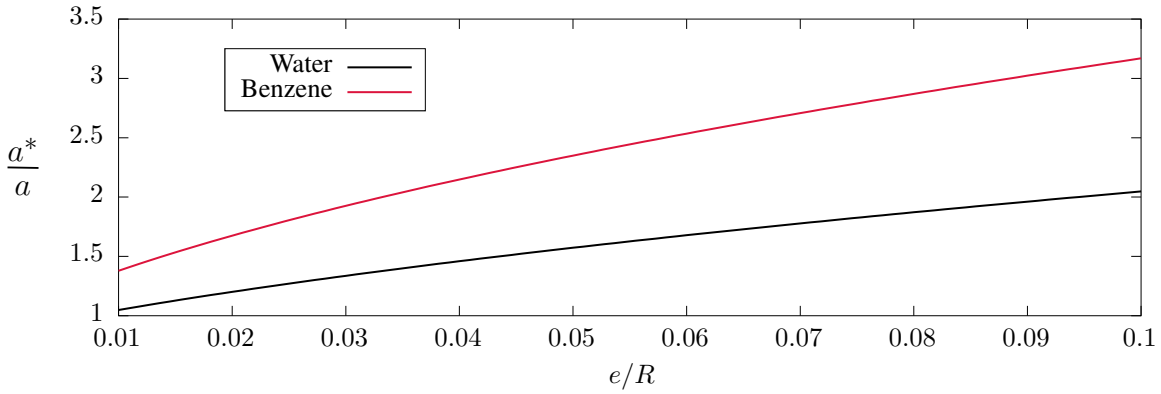

Figure 1. Wave speed ratio.

4.2 Grid Analysis

A grid analysis is conducted in order to ensure that the results obtained by the numerical procedure are not spurious and do not depend on the grid. We compute the normalized pressure at the valve as a function of the non-dimensional time using grids with different sizes, employing $\theta = 1$ and $\theta = 0.5$ for each grid and taking water to be the working fluid. Figures 2 and 3 show that the results become grid independent starting from $N = 5 \times 10^4$. Moreover, they also reveal that in order to reduce numerical uncertainty one needs to set $\theta = 1$, which denotes a first order implicit approximation in Eqs.(35) and (36).

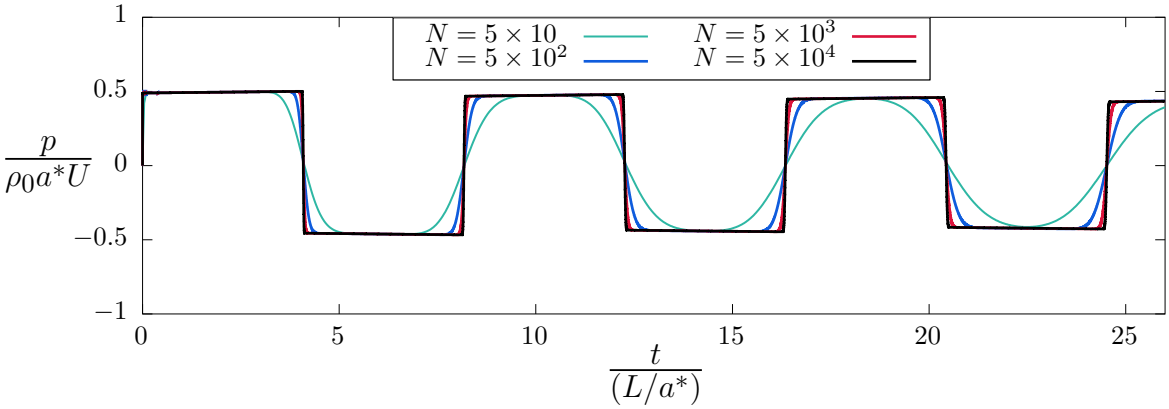

Figure 2. Pressure history at the valve for different grids with $\theta = 1$.

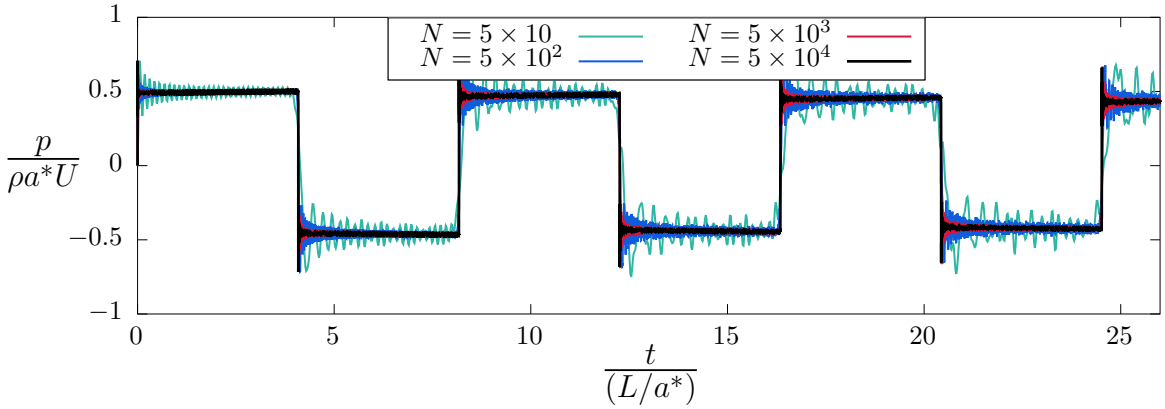

Figure 3. Pressure history at the valve for different grids with $\theta = 0.5$.

4.3 Pressure Response

We compare the normalized pressure values at the valve and at the pipe midpoint as a function of the non-dimensional time for different values of the ratio e/R. The simulations were performed with $N = 5 \times 10^4$ and $\theta = 1$ for water and benzene.

Results show that when the bulk viscosity coefficient is taken into account, the wave period is not equal to $4L/a^*$ - as one could expect since in the classical model the wave period is $4L/a$ - but instead it is explicitly dependent on the ratio e/R and on μ_b as reported in Figs.4-7, which reveal that the wave period increases as both the ratio e/R and μ_b increases. In analyzing the results for water in Figs.4 and 6 one can also see that when $e/R = 0.01$ the wave period gets close to the expected value of $4L/a^*$. Regarding the intensity of the pressure surges, Figs.4-7 show a decrease in the pressure amplitude as both the ratio e/R and μ_b increases. It is worth mentioning, for clarification sake, that the factor L/a^* employed in normalization of the time variable is computed for each curve in Figs. 4-7, therefore the x-axis of each curve is normalized employing its own wave speed a^*.

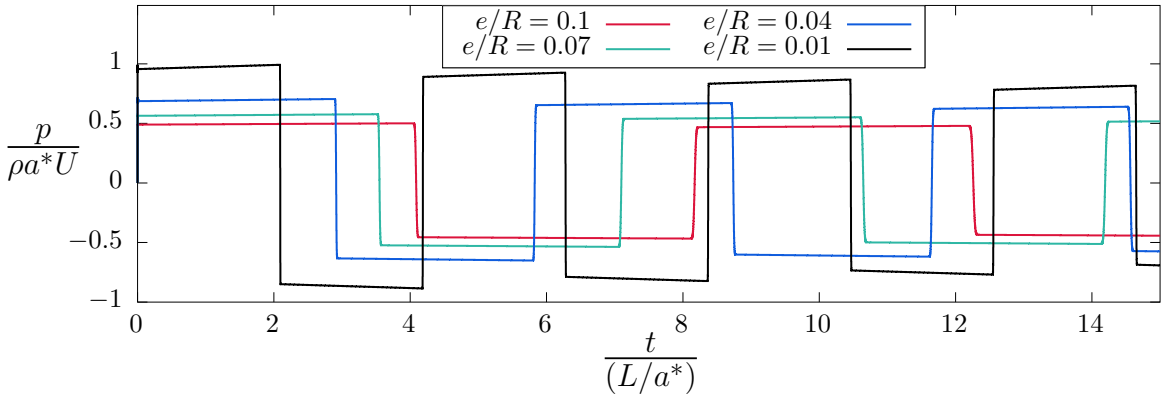

Figure 4. Pressure at the valve for different values of e/R ,working fluid: water.

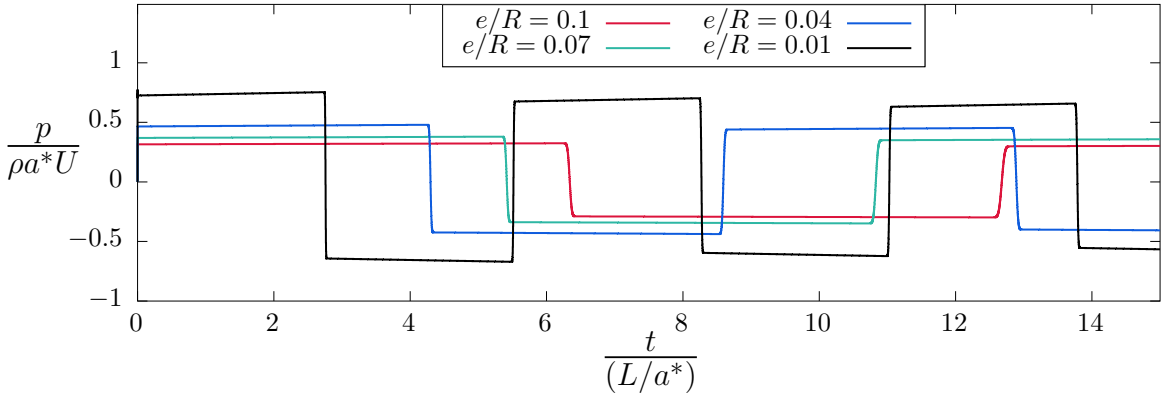

Figure 5. Pressure at the valve for different values of e/R ,working fluid: benzene.

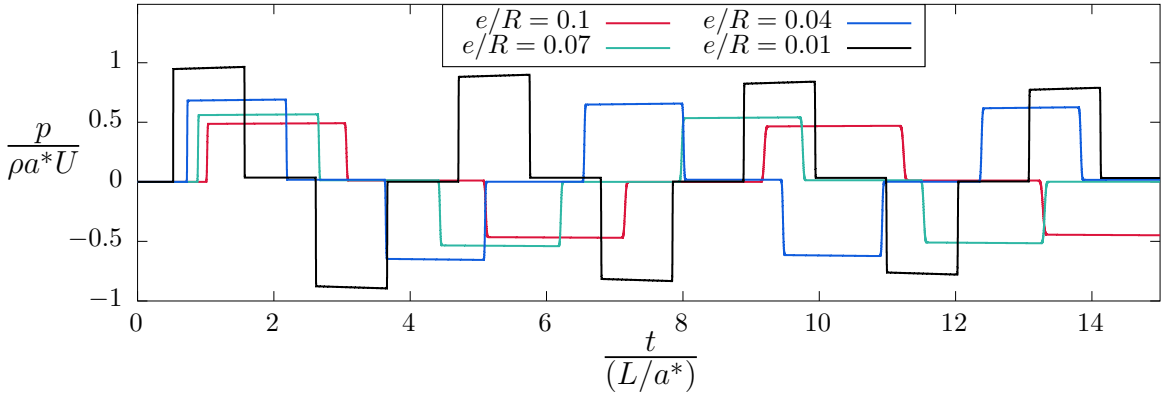

Figure 6. Pressure at the pipe midpoint for different values of e/R ,working fluid: water.

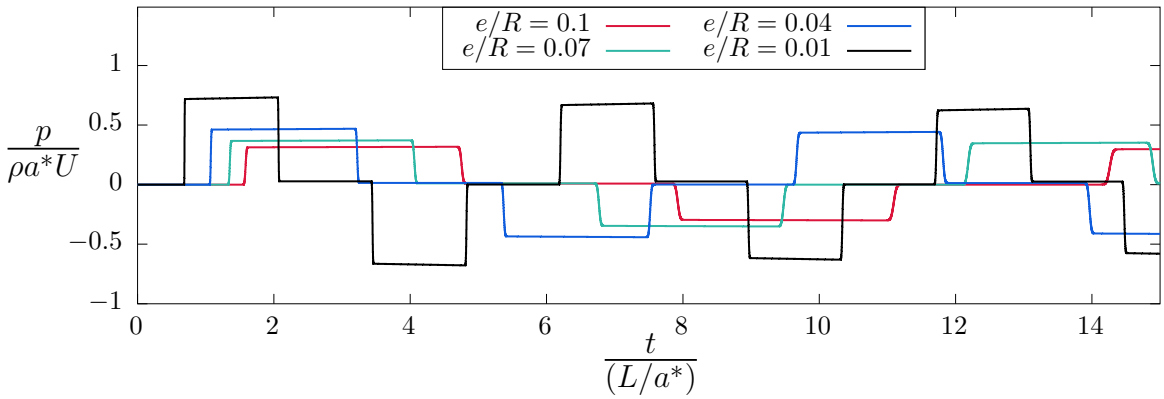

Figure 7. Pressure at the pipe midpoint for different values of e/R ,working fluid: benzene.

4.4 Energy Dissipation

Lastly, we conduct an energy analysis for benzene, water and for a fluid with intermediate value of bulk viscosity, while keeping the ratio $e/R = 0.01$. We employ Eq.(28) in order to assess the local rate of energy dissipation in the pipe midpoint due to both wall shear and bulk viscosity effects, as reported in Figs.8-10.

Results show the bulk viscosity effect manifests itself in the form of high intensity peaks of energy dissipation, taking place whenever the wavefront passes through the pipe midpoint and reducing intensity after each wave cycle. As it can be seen in Fig. 8, the value of the first peak can easily exceed the value of the energy dissipation due to wall shear stress. Figures 8-10 also show that the intensity of the dissipation peaks decreases as the bulk viscosity coefficient decreases, to a point that for water the energy dissipation due to bulk viscosity effects is negligible.

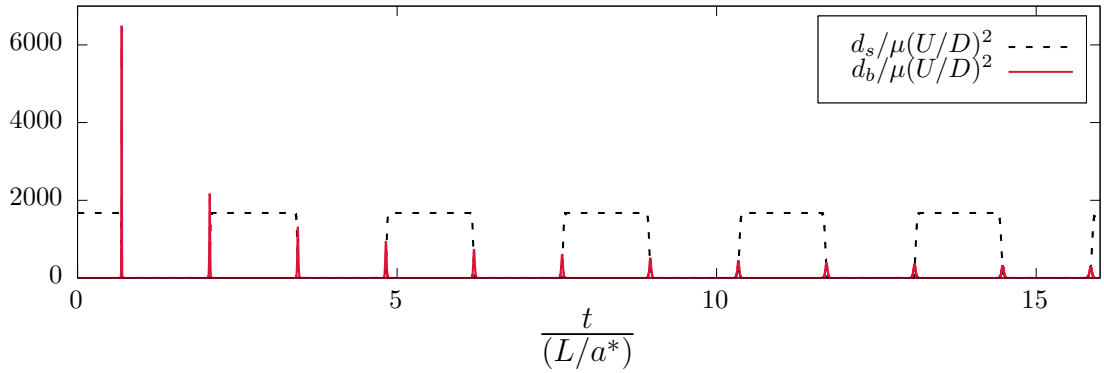

Figure 8. Energy dissipation at the pipe midpoint for benzene.

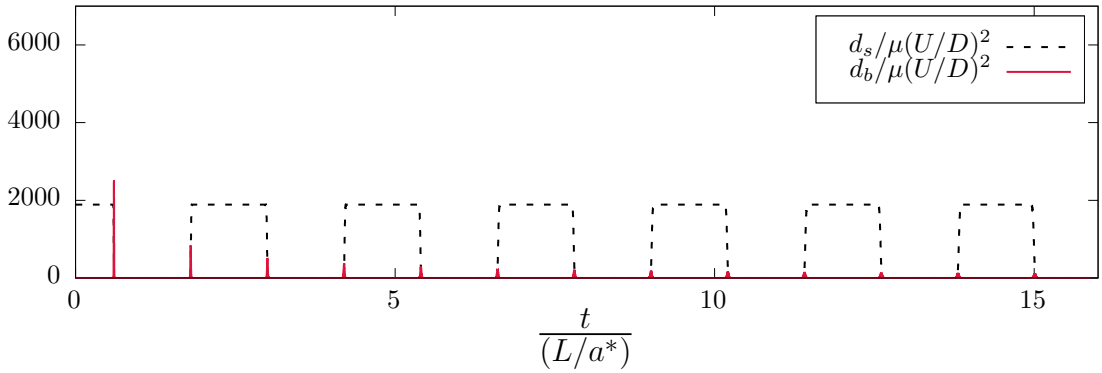

Figure 9. Energy dissipation at the pipe midpoint for a fluid with intermediate bulk viscosity.

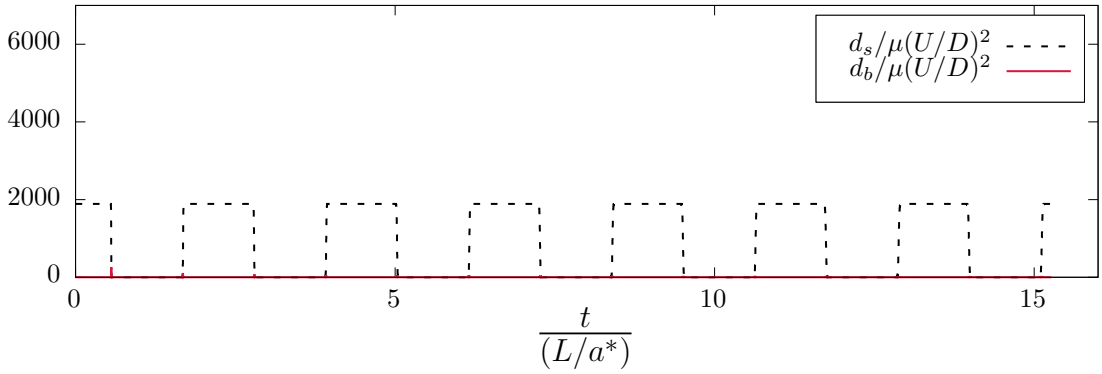

Figure 10. Energy dissipation at the pipe midpoint for water.

5. CONCLUDING REMARKS

A one-dimensional model taking into account the bulk viscosity coefficient has been developed and numerically studied in a resevoir-pipe-valve system with water-hammer generated by sudden valve closure. The model predicts an acoustic wave speed dependent on the bulk viscosity, typically greater than the wave speed in the classical water-hammer model. Numerical simulations were performed in order to assess the pressure response as well as the energy dissipation during the water-hammer event. It is found that large values of the bulk viscosity coefficient lead to an increase in the wave period. Regarding the energy analysis, the model predicts high intensity peaks of energy dissipation due to the bulk viscosity, easily exceeding the dissipation due to wall shear when considering large values of the bulk viscosity coefficient.

6. REFERENCES

Buresti, G., 2015. "A note on stokes' hypothesis". *Acta Mechanica*, Vol. 226, No. 10, pp. 3555–3559.

Chaudhry, M.H., 1979. "Applied hydraulic transients". Technical report, Springer.

Di Nucci, C. and Spena, A.R., 2016. "On transient liquid flow". *Meccanica*, Vol. 51, No. 9, pp. 2135–2143.

Dukhin, A.S. and Goetz, P.J., 2009. "Bulk viscosity and compressibility measurement using acoustic spectroscopy". *The Journal of chemical physics*, Vol. 130, No. 12, p. 124519.

Ghidaoui, M.S., Zhao, M., McInnis, D.A. and Axworthy, D.H., 2005. "A review of water hammer theory and practice". *Applied Mechanics Reviews*, Vol. 58, No. 1, pp. 49–76.

Gonzaga Filho, J.S., 2017. *Uma avaliação de modelos para descrever o atrito em escoamento unidimensional transiente*. Master's thesis, Universidade Federal Fluminense, Niterói, Brasil.

Landry, C., Nicolet, C., Bergant, A., Müller, A. and Avellan, F., 2012. "Modeling of unsteady friction and viscoelastic damping in piping systems". In *IOP Conference Series: Earth and Environmental Science*. IOP Publishing, Vol. 15, p. 052030.

Pezzinga, G., 2003. "Second viscosity in transient cavitating pipe flows". *Journal of Hydraulic Research*, Vol. 41, No. 6, pp. 656–665.

Rajagopal, K., 2013. "A new development and interpretation of the navier–stokes fluid which reveals why the "stokes assumption" is inapt". *International Journal of Non-Linear Mechanics*, Vol. 50, pp. 141–151.

Wylie, E.B., Streeter, V.L. and Suo, L., 1993. *Fluid transients in systems*, Vol. 1. Prentice Hall Englewood Cliffs, NJ.

7. RESPONSIBILITY NOTICE

The authors are solely responsible for the printed material included in this paper.